Deconvolution of Rashba and Dresselhaus spin-orbit coupling by crystal axis dependent measurements of coupled InAs/GaSb quantum wells

C. S. Knox,[1,2,*] L. H. Li,[1] M. C. Rosamond,[1] E. H. Linfield,[1] and C. H. Marrows[2]

[1]*School of Electronic and Electrical Engineering, University of Leeds, Leeds LS2 9JT, United Kingdom*
[2]*School of Physics and Astronomy, University of Leeds, Leeds LS2 9JT, United Kingdom*

The Dresselhaus spin-orbit interaction is expected to perturb the quantum spin Hall phase predicted to arise within InAs/GaSb coupled quantum wells. To gain a greater understanding of this interaction, the spin-orbit coupling in two InAs/GaSb coupled quantum well samples, grown along the [001] axis, was investigated along three different in-plane crystallographic axes. By measuring the crystallographic axis dependence of the Dresselhaus spin-orbit coupling, we can deconvolute this coupling from the spin splitting arising from axis-invariant Rashba spin-orbit coupling. We find that the Dresselhaus parameter is robust against an external gate bias and small changes in growth conditions, with an associated Dresselhaus parameter of $(0.20 \pm 0.08) \times 10^{-11}$ eV m being measured across all samples and top gate bias conditions. In addition, we show that the asymmetries associated with the coupled quantum well structure, leading to Rashba spin-orbit coupling, are likely to play a dominant role in determining the spin-orbit interaction experienced by a quantum spin Hall state as the system is tuned towards charge neutrality.

I. INTRODUCTION

The quantum spin Hall effect (QSHE) [1] is reminiscent of the integer quantum Hall effect [2,3]. However, instead of a single spin-degenerate edge state dominating transport under an applied external magnetic field (as is observed in the quantum Hall effect), a set of two, spin-filtered, counter-propagating edge states dominates transport in a system with unbroken time-inversion symmetry, with the spin polarization of these edge states directed out of the plane of the device [4].

In a material that exhibits the QSHE, there exists a bulk band gap that is topologically distinct from the vacuum. In order to bridge this gap, and so connect these topologically nontrivial and trivial regions of space, there must exist a set of gapless edge states, characterized by a Kramers doublet [5]. Due to the topological origin of these edge states, and the spin filtering they provide, the edge states are protected against elastic backscattering, as such scattering events would require a 180° spin flip.

Two material systems have been predicted to exhibit the QSHE: HgTe/CdTe quantum wells [6] and InAs/GaSb coupled quantum wells [5]. Both materials have exhibited charge transport dominated by helical edge states that are disrupted by the application of an external magnetic field [7,8], and both have shown the existence of some form of spin-polarized edge transport. In HgTe/CdTe quantum wells, this was demonstrated by the spontaneous generation of a spin current at the device edge, where the majority of spins are polarized out of the device plane [9]. In InAs/GaSb coupled quantum wells, spin-polarized edge transport was shown through study of Josephson junctions in which the InAs/GaSb was used as a nonsuperconducting spacer. In this case, devices showed superconducting quantum-interference-like behavior with a doubled periodicity compared to ordinary Cooper-pair mediated superconducting quantum interference devices, indicating that not only is transport dominated by edge states, but that there is also some separation of spin states along each channel edge [10]. In both cases, the interesting topology required for the effect to manifest itself arises from an inverted band gap, where the highest heavy hole valence band is more energetic than the lowest electron conduction band.

HgTe/CdTe and InAs/GaSb both have a zinc-blende crystal structure throughout their active regions, in which bulk inversion symmetry is broken. In addition, the stack structure of the InAs/GaSb coupled quantum well system adds another layer of asymmetry, known as structural inversion asymmetry. These asymmetries induce a potential gradient across the device, giving rise to an internal electric field that current carrying electrons will experience as an effective magnetic field. Such "magnetic" fields contribute to spin-orbit coupling (SOC), with bulk inversion asymmetry contributing to Dresselhaus SOC, and structural inversion asymmetry contributing to Rashba SOC. Crucially, these internal magnetic fields do not break time-inversion symmetry [11], and so can coexist with the QSHE [5].

However, as these SOC magnetic fields do not explicitly conserve out-of-plane spin [12], this coexistence leads to a perturbation of the QSHE edge states [13]. This has been predicted to change the normally completely out-of-plane polarized spins [see Fig. 1(a)] into k-dependent spin states [Fig. 1(b)], termed generic helical edge states [14,15]. It is worth noting that generic helical edge states are still protected against elastic backscattering, as this would require a 180° spin flip [14,15], as in the unperturbed case. Generic helical edge states do potentially, though, provide a perturbation that

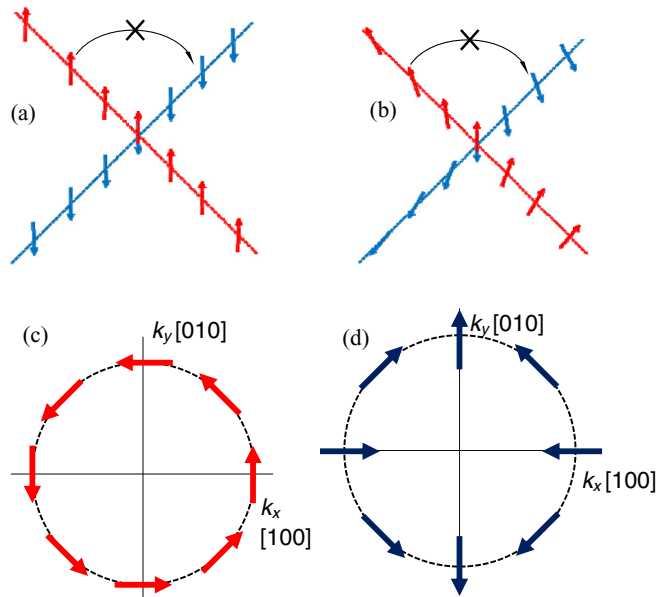*Corresponding author: py11csk@leeds.ac.uk

155323-1

FIG. 1. Schematic $E(k)$ diagram showing (a) unperturbed helical edge states, and (b) so-called generic helical edge states [14]. Spin-up states are shown in red and spin-down states in blue, with a forbidden elastic backscattering event highlighted (black arrow). Note that to undergo elastic backscattering within a generic helical edge state, a 180° spin flip is still required. (c,d) are schematics of the 2D Fermi circle (dotted) showing spin-splitting magnetic fields that arise due to Rashba SOC (red arrows), and the Dresselhaus SOC (blue arrows), respectively, for various crystallographic axes.

would enable easier inelastic backscattering processes, hence disrupting the quantized nature of the conductance in the QSHE.

The Dresselhaus [15] and Rashba [14] SOC terms contribute in different ways to the production of generic helical edge states, making the deconvolution of these two functionally similar parameters of experimental interest. In particular, the k-linear, electron dominated Rashba term does not contribute to the disruption of the perfect out-of-plane polarization, although higher-order terms dominated by heavy holes would be significant [13,14]. The electric field responsible for the Rashba SOC will always lie along the growth direction. Thus, in wafers grown along the [001] axis, it will always be perpendicular to the current, and so the spin splitting caused by the internal field will have a constant magnitude across all crystallographic axes [see Fig. 1(c)]. However, for Dresselhaus SOC, as the crystalline asymmetry, and therefore the electric field that gives rise to SOC, are dependent on the crystal structure, the spin-splitting field experienced by the current carrying electrons will vary from axis to axis [see Fig. 1(d)] [16,17]. This angular dependence can thus be used to separate the crystallographic axis-invariant Rashba SOC from the axis dependent Dresselhaus SOC.

Here we report on the relative magnitudes of the Dresselhaus and k-linear Rashba SOCs in an InAs/GaSb QHSE candidate by measuring two similar wafers of comparable electrical quality. In one case, charge transport arises from a single carrier gas; in the other case, both the electronlike carrier density localized in the InAs layer and the holelike

carrier density within the GaSb layer make a significant contribution to transport. In this way we show that not only is the Dresselhaus parameter constant across all top gate bias conditions, as expected, but it is also robust against variations in sample properties arising from small changes in the growth conditions. Additionally, the much larger Rashba parameter increases as carriers are depleted from the active region, implying that the internal potential gradient caused by the epitaxial (stack) structure is instrumental to the SOC observed.

II. EXPERIMENT

The layer structure of the InAs/GaSb heterostructures is shown in Fig. 2(a), with wafer 2 having a 4-μm, rather than 3-μm, GaSb buffer in an otherwise identical structure. Both wafers were grown by solid source molecular beam epitaxy in the [001] direction on a (001) n^+ GaAs substrate, but with wafer 2 having a slightly lower arsenic overpressure when compared with wafer 1 (3.4×10^{-6} mbar, compared with 4.5×10^{-6} mbar) during the InAs growth.

Wafers were patterned into 50-μm-wide Hall bars, with 250-μm gaps between probe arms, using optical lithography and wet chemical etching [18], after first depositing Cr/Au Ohmic contacts using thermal evaporation. A 30-nm-thick Al_2O_3 dielectric was then deposited by atomic layer deposition at 200 °C on top of the Hall bar, with a Cr/Au top gate electrode subsequently formed using thermal evaporation. An optical micrograph of a typical device is shown in Fig. 2(b). Measurements were undertaken between 0 and 8 T in a continuous flow helium cryostat at 1.5 K, using standard lock-in techniques, with a source-drain current of 1 μA.

Hall resistance data for each wafer, at zero top gate bias, are shown in Figs. 3(a) and 3(b). Wafer 1 shows well-quantized quantum Hall plateaus at even-integer multiples of the von Klitzing constant at most field values [19]. In contrast, wafer 2 shows a slight bending in the low-field Hall trace (<1 T), in addition to plateaus quantized at odd-integer multiples of the von Klitzing constant. The latter is taken to indicate the presence of hybridization between a two-dimensional (2D) electron gas localized in the InAs layer and a 2D hole gas within the active GaSb layer [20] that is not present in wafer 1. Despite this, both wafers showed transport behavior dominated by electrons, as indicated by the sign of the low-field (<0.2 T) Hall coefficient. In addition, all measured samples showed Shubnikov–de Haas (SdH) oscillations that are contained within a single envelope function with a unified temperature dependence up to 10 K (not shown here), from which the effective mass could be extracted [21]. This confirms that the magnetoresistance behavior is dominated by a single carrier species (electrons) within this regime [21,22]. A summary of the zero top gate bias transport properties for both wafers is displayed in Table I.

Magnetoresistance measurements were then performed for different gate biases between ±1 V at 1.5 K with the current applied parallel to the [010] crystallographic axis. It is worth noting that once a top gate bias of greater than ±1 V is applied, hysteretic behavior is observed—the zero top gate bias magnetotransport is then different from the as-cooled state, with SdH oscillations no longer contained in a single envelope function. This is possibly caused by charge traps
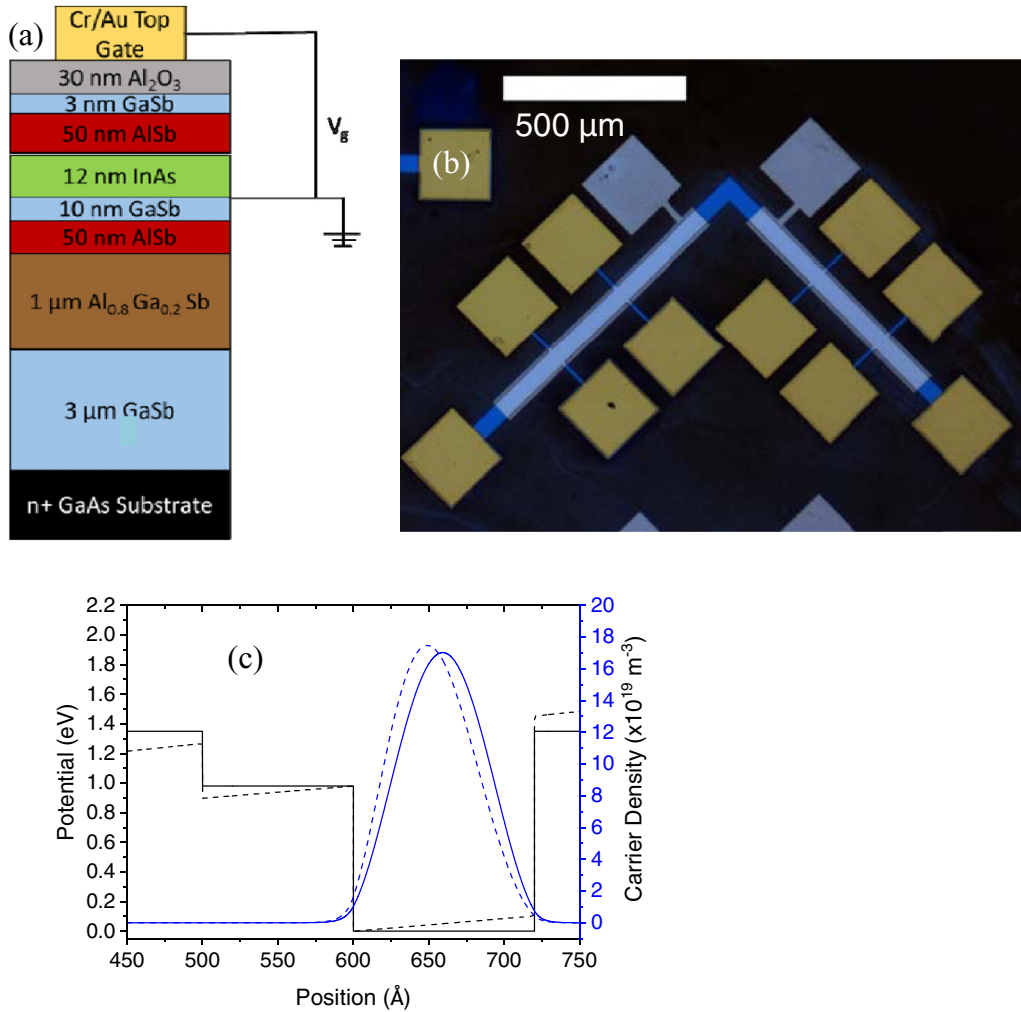
FIG. 2. (a) Heterostructure design for wafer 1; wafer 2 is identical, except for the use of a 4-μm-thick GaSb buffer layer. Note that, since the InAs layer is closer to the top surface, the top gate modulates the electron carrier density. (b) Optical micrograph of a typical right-angled Hall bar used in this study. (c) Calculated conduction band diagrams [39,40] (black lines) and electron distributions at a fixed carrier density (blue lines) at 0 applied bias (solid lines) and -100 kV/cm electric field, corresponding to approximately a -1 V applied top gate bias (dashed lines). Here, the zero in energy is defined as being at the bottom of the InAs conduction band.

underneath the quantum well which results in a second carrier contributing to transport. As such, we are unable to tune the system into a charge-neutral state, where topologically nontrivial transport would dominate [8]. Below a ± 1 V top gate bias, however, one can assume that only the carrier density in the InAs layer is being modulated, with all other layers screened from the applied top gate bias.

A discrete Fourier transform of the observed SdH oscillations, plotted against inverse field, was analyzed and two distinct peaks observed at almost all top gate biases. An example of the oscillations, at gate biases of 0 and -1 V, is shown in Fig. 3(c), with the associated discrete Fourier transform presented in Fig. 3(d). We equate the frequencies associated with the two observed peaks to a spin-split carrier density, the higher of which is aligned to the spin-splitting field caused by the SOC within the material [23,24]. This was repeated across three more devices, along the [100], [110], and [1$\bar{1}$0] crystallographic axes, respectively, and repeated on a similar set of devices from wafer 2.

III. FURTHER ANALYSIS AND DISCUSSION

Since the SdH oscillations appear to be due to a single carrier species, they can be analyzed using the expression [23]

$$\Omega = \frac{(n^+ - n^-)\hbar^2}{m^*}\sqrt{\frac{\pi}{2(n^+ + n^-) - 2(n^+ - n^-)}}, \quad (1)$$

where n^+ and n^- are the carrier densities associated with the aligned and antialigned peaks, respectively; m^* is the effective mass; and Ω is the total SOC parameter.

Above a $+0.2$ V applied top gate bias, a new set of SdH oscillations appears with an entirely different envelope function, along with an additional peak in the Fourier transform. We take this to be indicative of occupation of a second electron subband, and as such, our model for spin-orbit coupling is no longer valid [24], as intersubband scattering does not conserve spin. Furthermore, as the population of the upper subband increases, intersubband scattering will play an increasingly significant part in the spin relaxation [25], masking the effects
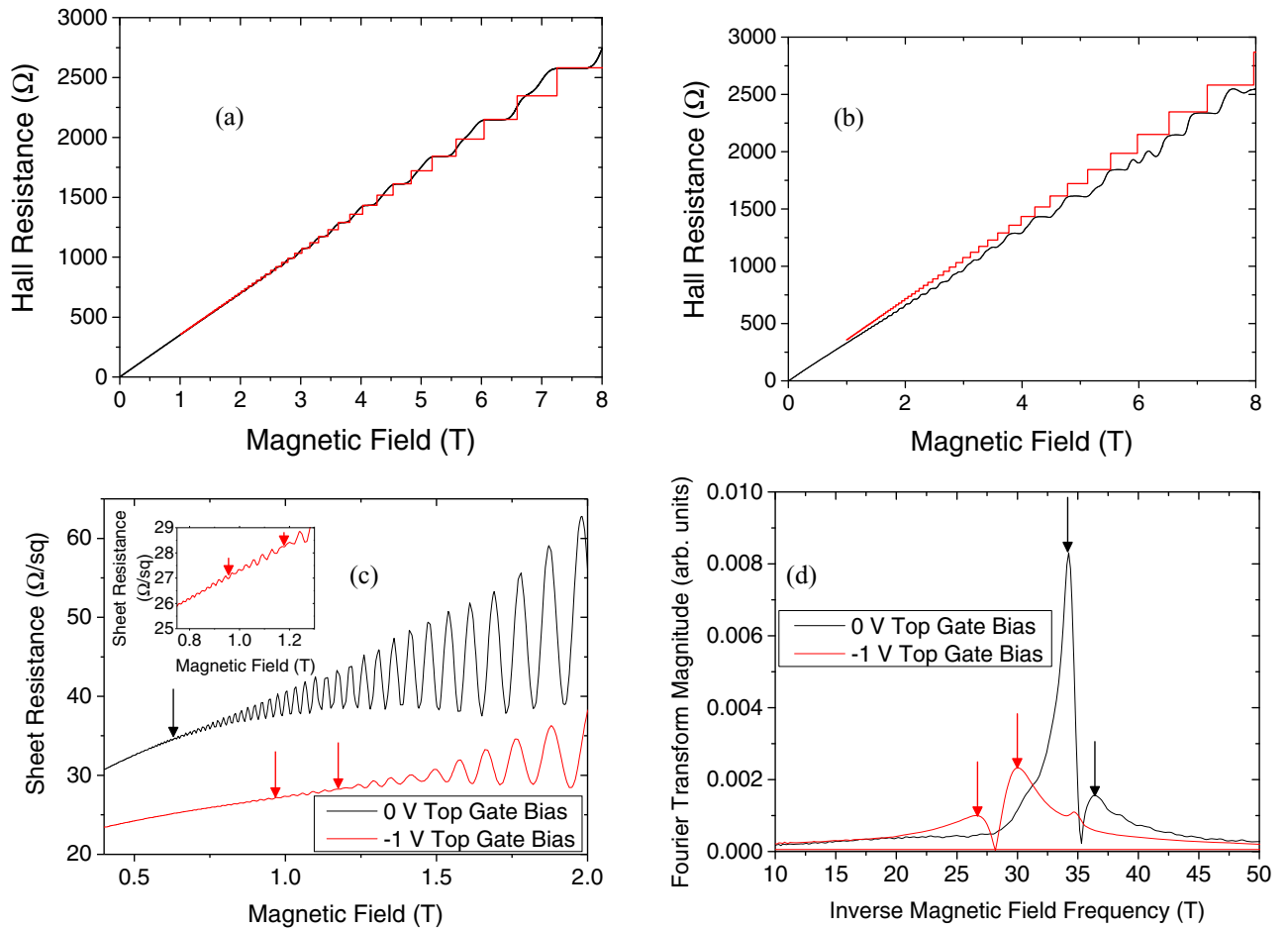
FIG. 3. (a,b) Hall resistance data for wafers 1 and 2, respectively. The red traces in (a,b) are the expected plateaus arising from the integer quantum Hall effect, and are calculated using the carrier density determined from the low-field (<0.2 T) Hall effect. (c) SdH oscillations for wafer 2 along the [010] axis, for both 0 and -1 V top gate biases. Beating nodes, indicating the presence of two distinct frequencies, are marked with arrows. Inset: expanded version of the magnetotransport at a -1 V bias, highlighting the beating nodes. (d) Discrete Fourier transform of both sets of oscillations in (c), showing two distinct frequencies for each (marked with arrows).

of Rashba and Dresselhaus SOC. Therefore, we neglect data taken at gate biases more positive than $+0.2$ V in our analysis.

The SOC parameter, Ω, is plotted in Fig. 4(a) as a function of gate bias along different crystallographic axes. As illustrated in Fig. 1(d), the Dresselhaus spin-splitting field is parallel to the current direction when the current is applied along the [100] and [010] axes, and so should have a negligible effect on the observed spin splitting [16]. As such, since we find experimentally equal SOC parameters when the current is applied along the [100] and [010] axes, we plot a single set of SOC parameters representing these two axes.

TABLE I. Table of zero top gate bias transport parameters for wafer 1 and wafer 2 for current applied parallel to the [100] axis.

Wafer	Carrier density (cm^{-2})	Sheet mobility (cm^2 V^{-2} s^{-1})	Effective mass (m_0)
Wafer 1	$(17.5 \pm 0.2) \times 10^{11}$	$111\,000 \pm 1000$	0.040 ± 0.005
Wafer 2	$(17.6 \pm 0.2) \times 10^{11}$	$137\,000 \pm 1000$	0.032 ± 0.005

The total SOC parameter increases as the top gate bias is made more negative for measurements along all crystallographic axes. While there is a small increase in the difference between the carrier densities associated with the spin-orbit field aligned and antialigned peaks (i.e., $n^+ - n^-$) in the discrete Fourier transformed SdH oscillations as the top gate bias becomes more negative, the main reason for this trend appears to be the drop in carrier density associated with depletion of electrons from the InAs layer. This would signify that a greater proportion of the electrons become aligned with the total SOC field as the top gate bias becomes more negative.

We interpret this increase in the SOC parameter with more negative top gate bias by reasoning that the inherent asymmetry associated with the stacked heterostructure will provide some built-in electric field [24,26], and thus contribute to all terms in the Rashba SOC [16,27,28]. Specifically, since the intrinsically p-type GaSb is underneath the intrinsically n-type InAs layer [29], a dipole will be formed across the active layers. By applying a negative top gate bias and making the top of the stack structure more negative, the electric field that arises from the applied top gate bias will enhance the internal field, resulting in the observed behavior. A schematic
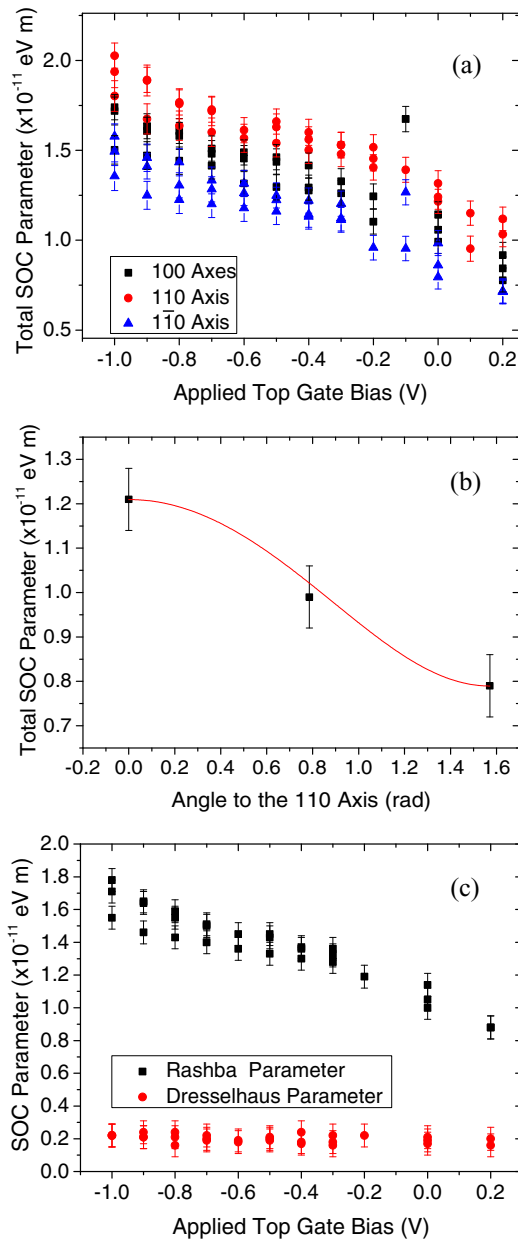
FIG. 4. (a) SOC parameters along the [100], [110], and [1$\bar{1}$0] axes of wafer 1, plotted as a function of top gate bias. (b) Total SOC parameter at zero top gate bias in wafer 1, plotted as a function of angle to the [110] axis, showing the expected $\cos 2\theta$ dependence. The fit to Eq. (2) is shown in red. (c) Rashba and Dresselhaus parameters extracted from fitting Eq. (2) to the relevant data in (a).

the second case, a subtractive effect. Thus, we can deconvolute these two SOC terms by fitting the crystallographic axis dependence of the total SOC parameter to the following expression [16]:

$$\Omega = \sqrt{\alpha^2 + \beta^2 + 2\alpha\beta\cos 2\theta}, \qquad (2)$$

where α is the total Rashba parameter, β is the total Dresselhaus parameter, and θ is the angle between the direction of the current and the [110] axis. This fit, for the case of zero gate bias, is shown in Fig. 4(b). As the total SOC parameter, Ω, is experimentally identical for the [100] and [010] axes, there is confidence that the observed values of Ω along the [110] and [1$\bar{1}$0] axes are the maximum and minimum values for Ω, respectively, due to the $\cos(2\theta)$ term in Eq. (2).

A plot of the two contributions to the total SOC extracted by this method is shown in Fig. 4(c) as a function of applied top gate bias. As expected, the fitted Rashba parameter matches closely to the total SOC observed for the [100] and [010] axes, where the Dresselhaus contribution would be expected to be negligible and the Rashba term makes a dominant contribution to the SOC, as seen in previous studies [16,30]. The data also fit well to the gate dependences observed along each of the axes.

The Rashba parameter was calculated to vary between $(0.88 \pm 0.07) \times 10^{-11}$ eV m at 0.2 V applied top gate bias and $(1.78 \pm 0.07) \times 10^{-11}$ eV m at -1.0 V applied bias. This is significant, as typical measurements on InAs quantum wells with a doped underlayer (to supply the structural inversion asymmetry needed for the Rashba SOC) place the maximum measured Rashba parameter to be approximately 1×10^{-11} eV m [16,26]. We reason that the presence of a GaSb layer integrated into the active portion of the quantum well induces a greater asymmetry within the quantum well when compared to dopants that are remote to the transport channel.

The Dresselhaus parameter was calculated to be $(0.20 \pm 0.07) \times 10^{-11}$ eV m for all gate biases. At zero gate bias, this would result in a spin-splitting energy due to the Dresselhaus spin-orbit coupling of 1.3 ± 0.5 meV [26]. Interestingly, this is close to the predicted value of the splitting due to bulk-inversion asymmetry in HgTe/CdTe quantum wells and InAs/GaSb coupled quantum wells of 1.6 meV [31,32].

We repeated these sets of measurements on wafer 2, in the two-carrier regime, and the results are plotted in Fig. 5. It is worth remarking that although this wafer is in the two-carrier regime, the transport is still electron dominated, and we are unable to tune through a hybridization gap. We thus neglect the effect of any sort of topologically nontrivial behavior or higher-order Rashba terms.

Despite the lower effective mass in wafer 2, as shown in Table I, the Dresselhaus parameter for this wafer, $(0.19 \pm 0.08) \times 10^{-11}$ eV m, was seen to be similar to that obtained in wafer 1. The only difference between the two wafers is the elevated Rashba parameter in wafer 2, which we attribute to a greater contribution to the internal electric field from the hole gas within the GaSb layer—a more highly charged GaSb layer would result in a steeper potential gradient across the coupled quantum well structure, resulting in a larger Rashba parameter.
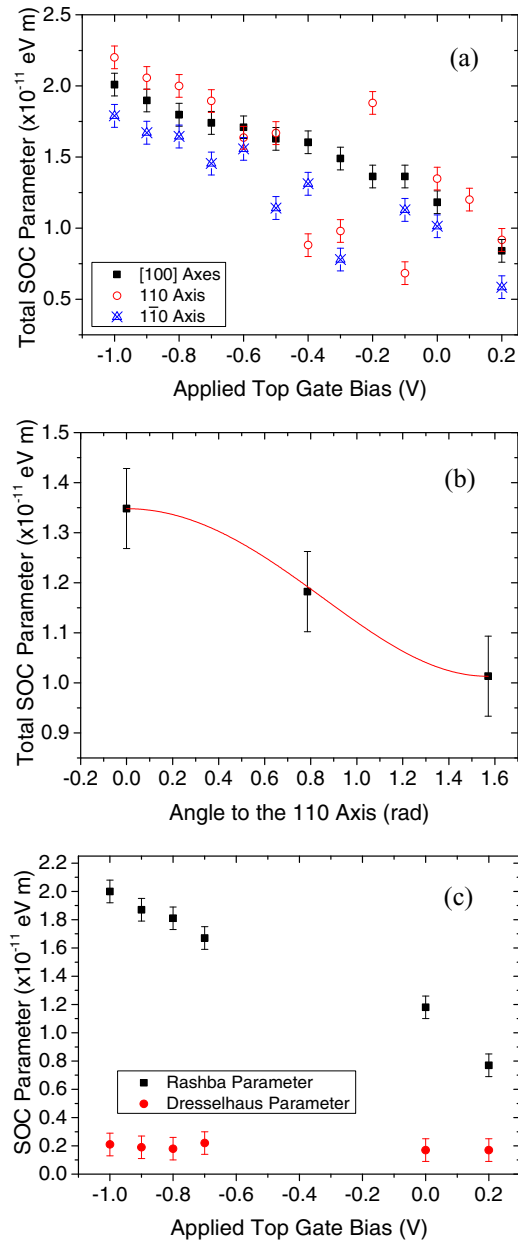
diagram of this is shown in Fig. 2(c), with the carrier density within the InAs layer moving closer to the GaSb layer as the top of the heterostructure is made more negative.

In Fig. 4(a), measurements along the [110] axis are seen to have a larger SOC parameter compared with measurements along the [100] and [010] axes. Conversely, measurements along the [1$\bar{1}$0] axis show a smaller SOC parameter when compared to the [100] and [010] axes. This is expected, as in the first case the Dresselhaus spin-splitting field will have an additive contribution to the Rashba spin splitting, and in

FIG. 5. (a) SOC parameters along the [100], [110], and [1$\bar{1}$0] axes of wafer 2, plotted as a function of top gate bias. (b) Total SOC parameter at zero top gate bias in wafer 2, plotted as a function of angle to the [110] axis, showing the expected cos 2θ dependence. The fit to Eq. (2) is shown in red. (c) Rashba and Dresselhaus parameters extracted from fitting Eq. (2) to the data in the relevant parts of (a).

IV. CONCLUSION

We have investigated the SOC within InAs/GaSb coupled quantum wells along different crystallographic axes in both the -single- and double-carrier, electron-dominated regimes, and explicitly deconvoluted the Rashba and Dresselhaus terms as a function of gate bias.

We find that the k-linear Rashba SOC is sensitive to top gate bias conditions, and the precise heterostructure growth. We determine values for the Rashba parameter varying between $(0.88 \pm 0.07) \times 10^{-11}$ eV m and $(1.78 \pm 0.07) \times 10^{-11}$ eV m at 0.2 V and -1.0 V, respectively,

in wafer 1, and $(0.77 \pm 0.08) \times 10^{-11}$ eV m and $(2.00 \pm 0.08) \times 10^{-11}$ eV m at similar top gate biases in wafer 2.

In contrast, the Dresselhaus SOC is constant across all top gate biases. In addition, it appears insensitive to small variations in sample properties arising from changes in the growth conditions, as our value of $(0.20 \pm 0.07) \times 10^{-11}$ eV m in the single-carrier regime aligns well with our measurements in the double-carrier regime. Our data also agree well with recent measurements by Arjan *et al.* on a wafer with a similar stack structure, but where the SOC parameters were extracted from fitting the beating modes in the SdH oscillations as a function of top gate bias [30]. This is, however, only possible when using samples with a very high carrier density or an exceptional mobility, when many beating modes due to SOC can be seen at an extremely low magnetic field. It would be masked in samples with comparatively low mobility [33], and does not enable explicit deconvolution of the Rashba and Dresselhaus terms and their gate dependence.

Recent measurements on strained InAs/GaInSb coupled quantum wells [34] and InAs/GaSb coupled quantum wells mounted on piezoelectric stressors [35] have highlighted the tunability of the hybridization gap with either applied or growth-related strain effects. In addition, the Dresselhaus and Rashba spin-orbit coupling strength in bulk semiconductors are both tunable by applied stress, leading to a deformation of the crystal structure [36]. This opens up the possibility that the topological behavior observed in these classes of structures could be significantly modified by strain tuning.

In this work, we have not been able to study SOC close to the hybridization gap, where topological behavior will begin to have a significant effect on transport. However, the technique discussed here may not then be applicable owing to (1) the low electron-like carrier density as the hybridization gap is approached and (2) the resonant behavior of the sample resistance within a gapped regime. In addition (3), due to the comparable carrier densities of electrons and holes within the heterostructure as the topologically interesting region is approached, additional spin relaxation mechanisms are expected to be apparent [37,38], independent of the SOC within the material. Future studies in this regime would, however, provide fascinating insights into the nature of the topological state seen in this class of material. Furthermore, the internal electric fields within the material could be engineered, e.g., by swapping positions of the active InAs and GaSb layers, changing quantum well thicknesses, or adjusting their carrier densities, enabling tailoring of spin-orbit coupling in the topological regime.

The data associated with this paper are publicly available from the University of Leeds Data Repository (see Ref. [41]).

[1] C. L. Kane and E. J. Mele, Z_2 Topological Order and the Quantum Spin Hall Effect, Phys. Rev. Lett. **95**, 146802 (2005).

[2] D. J. Thouless, M. Kohmoto, M. P. Nightingale, and M. Dennijs, Quantized Hall Conductance in a Two-Dimensional Periodic Potential, Phys. Rev. Lett. **49**, 405 (1982).

[3] K. Vonklitzing, G. Dorda, and M. Pepper, New Method for High-Accuracy Determination of the Fine-Structure Constant Based on Quantized Hall Resistance, Phys. Rev. Lett. **45**, 494 (1980).

[4] C. L. Kane and E. J. Mele, Quantum Spin Hall Effect in Graphene, Phys. Rev. Lett. **95**, 226801 (2005).

[5] C. X. Liu, T. L. Hughes, X. L. Qi, K. Wang, and S. C. Zhang, Quantum Spin Hall Effect in Inverted Type-II Semiconductors, Phys. Rev. Lett. **100**, 236601 (2008).

[6] B. A. Bernevig, T. L. Hughes, and S. C. Zhang, Quantum spin Hall effect and topological phase transition in HgTe quantum wells, Science **314**, 1757 (2006).

[7] M. Konig, S. Wiedmann, C. Brune, A. Roth, H. Buhmann, L. W. Molenkamp, X. L. Qi, and S. C. Zhang, Quantum spin Hall insulator state in HgTe quantum wells, Science **318**, 766 (2007).

[8] T. X. Li, P. Wang, H. Fu, L. Du, K. A. Schreiber, X. Mu, X. Liu, G. Sullivan, G. A. Csáthy, X. Lin *et al.*, Observation of a Helical Luttinger Liquid in InAs/GaSb Quantum Spin Hall Edges, Phys. Rev. Lett. **115**, 136804 (2015).

[9] C. Brune, A. Roth, H. Buhmann, E. M. Hankiewicz, L. W. Molenkamp, J. Maciejko, X. L. Qi, and S. C. Zhang, Spin polarization of the quantum spin Hall edge states, Nat. Phys. **8**, 485 (2012).

[10] V. S. Pribiag, A. J. A. Beukman, F. Qu, M. C. Cassidy, C. Charpentier, W. Wegscheider, and L. P. Kouwenhoven, Edge-mode superconductivity in a two-dimensional topological insulator, Nat. Nanotechnol. **10**, 593 (2015).

[11] G. Tkachov and E. M. Hankiewicz, Spin-helical transport in normal and superconducting topological insulators, Phys. Status Solidi B **250**, 215 (2013).

[12] S. D. Ganichev and L. E. Golub, Interplay of Rashba/Dresselhaus spin splittings probed by photogalvanic spectroscopy—A review, Phys. Status Solidi B **251**, 1801 (2014).

[13] D. G. Rothe, R. W. Reinthaler, C. X. Liu, L. W. Molenkamp, S. C. Zhang, and E. M. Hankiewicz, Fingerprint of different spin-orbit terms for spin transport in HgTe quantum wells, New J. Phys. **12**, 065012 (2010).

[14] L. Ortiz, R. A. Molina, G. Platero, and A. M. Lunde, Generic helical edge states due to Rashba spin-orbit coupling in a topological insulator, Phys. Rev. B **93**, 205431 (2016).

[15] A. Rod, T. L. Schmidt, and S. Rachel, Spin texture of generic helical edge states, Phys. Rev. B **91**, 245112 (2015).

[16] Y. H. Park, H. J. Kim, J. Chang, S. H. Han, J. Eom, H. J. Choi, and H. C. Koo, Separation of Rashba and Dresselhaus spin-orbit interactions using crystal direction dependent transport measurements, Appl. Phys. Lett. **103**, 252407 (2013).

[17] S. D. Ganichev, V. V. Bel'kov, L. E. Golub, E. L. Ivchenko, P. Schneider, S. Giglberger, J. Eroms, J. De Boeck, G. Borghs, W. Wegscheider *et al.*, Experimental Separation of Rashba and Dresselhaus Spin Splittings in Semiconductor Quantum Wells, Phys. Rev. Lett. **92**, 256601 (2004).

[18] A. N. Pal, S. Muller, T. Ihn, K. Ensslin, T. Tschirky, C. Charpentier, and W. Wegscheider, Influence of etching processes on electronic transport in mesoscopic InAs/GaSb quantum well devices, AIP Adv. **5**, 077106 (2015).

[19] S. W. Hwang, H. P. Wei, L. W. Engel, D. C. Tsui, and A. M. M. Pruisken, Scaling in spin-degenerate Landau levels in the integer quantum Hall effect, Phys. Rev. B **48**, 11416 (1993).

[20] K. Suzuki, S. Miyashita, and Y. Hirayama, Transport properties in asymmetric InAs/AlSb/GaSb electron-hole hybridized systems, Phys. Rev. B **67**, 195319 (2003).

[21] Y. F. Komnik, V. V. Andrievskii, I. B. Berkutov, S. S. Kryachko, M. Myronov, and T. E. Whall, Quantum effects in hole-type Si/SiGe heterojunctions, Low Temp. Phys. **26**, 609 (2000).

[22] C. S. Knox, C. Morrison, F. Herling, D. A. Ritchie, O. Newell, M. Myronov, E. H. Linfield, and C. H. Marrows, Partial hybridisation of electron-hole states in an InAs/GaSb double quantum well heterostructure, Semicond. Sci. Technol. **32**, 104002 (2017).

[23] D. Grundler, Large Rashba Splitting in InAs Quantum Wells due to Electron Wave Function Penetration into the Barrier Layers, Phys. Rev. Lett. **84**, 6074 (2000).

[24] G. Engels, J. Lange, T. Schapers, and H. Luth, Experimental and theoretical approach to spin splitting in modulation-doped $In_xGa_{1-x}As$/InP quantum wells for $B \rightarrow 0$, Phys. Rev. B **55**, R1958 (1997).

[25] H. Luo, X. Qian, X. Ruan, Y. Ji, and V. Umansky, Spin dynamics of electrons in the first excited subband of a high-mobility low-density two-dimensional electron system, Phys. Rev. B **80**, 193301 (2009).

[26] J. Nitta, T. Akazaki, H. Takayanagi, and T. Enoki, Gate Control of Spin-Orbit Interaction in an Inverted $In_{0.53}Ga_{0.47}As$/$In_{0.52}Al_{0.48}As$ Heterostructure, Phys. Rev. Lett. **78**, 1335 (1997).

[27] G. Gumbs, Rashba effect on the plasma oscillations in a coupled bilayer of electrons and holes, Appl. Phys. Lett. **85**, 2821 (2004).

[28] A. H. A. Hassan, R. J. H. Morris, O. A. Mironov, S. Gabani, A. Dobbie, and D. R. Leadley, An origin behind Rashba spin splitting within inverted doped sGe heterostructures, Appl. Phys. Lett. **110**, 042405 (2017).

[29] H. Kroemer, The 6.1 angstrom family (InAs, GaSb, AlSb) and its heterostructures: A selective review, Phys. E (Amsterdam) **20**, 196 (2004).

[30] F. K. d. V. Arjan, J. A. Beukman, J. van Veen, R. Skolasinski, and M. Wimmer, Spin-orbit interaction in a dual gated InAs/GaSb quantum well, Phys. Rev. B **96**, 241401 (2017).

[31] M. Konig, H. Buhmann, L. W. Molenkamp, T. Hughes, C. X. Liu, X. L. Qi, and S. C. Zhang, The quantum spin Hall effect: Theory and experiment, J. Phys. Soc. Jpn. **77**, 031007 (2008).

[32] P. C. Klipstein, Structure of the quantum spin Hall states in HgTe/CdTe and InAs/GaSb/AlSb quantum wells, Phys. Rev. B **91**, 035310 (2015).

[33] B. M. Nguyen, W. Yi, R. Noah, J. Thorp, and M. Sokolich, High mobility back-gated InAs/GaSb double quantum well grown on GaSb substrate, Appl. Phys. Lett. **106**, 032107 (2015).

[34] L. J. Du, T. Li, W. Lou, X. Wu, X. Liu, Z. Han, C. Zhang, G. Sullivan, A. Ikhlassi, K. Chang *et al.*, Tuning Edge States in Strained-Layer InAs/GaInSb Quantum Spin Hall Insulators, Phys. Rev. Lett. **119**, 056803 (2017).

[35] L. Tiemann, S. Mueller, Q. S. Wu, T. Tschirky, K. Ensslin, W. Wegscheider, M. Troyer, A. A. Soluyanov, and T. Ihn, Impact of strain on the electronic properties of InAs/GaSb quantum well systems, Phys. Rev. B **95**, 115108 (2017).

[36] B. A. Bernevig and S. C. Zhang, Spin splitting and spin current in strained bulk semiconductors, Phys. Rev. B **72**, 115204 (2005).

[37] J. S. Sandhu, A. P. Heberle, J. J. Baumberg, and J. R. A. Cleaver, Gateable Suppression of Spin Relaxation in Semiconductors, Phys. Rev. Lett. **86**, 2150 (2001).

[38] G. L. Bir, A. G. Aronov, and G. E. Pikus, Spin relaxation of electrons scattered by holes, Zh. Eksp. Teor. Fiz. **69**, 1382 (1975).

[39] P. Harrison and A. Valavanis, in *Quantum Wells, Wires and Dots: Theoretical and Computational Physics of Semiconductor Nanostructures* (John Wiley & Sons, Chichester, UK, 2016), pp. 19–81.

[40] C. E. Pryor and M.-E. Pistol, Band-edge diagrams for strained III–V semiconductor quantum wells, wires, and dots, Phys. Rev. B **72**, 205311 (2005).

[41] C. S. Knox, L. H. Li, M. C. Rosamond, E. H. Linfield, and C. H. Marrows, Dataset Associated with 'Deconvolution of Rashba and Dresselhaus spin-orbit coupling by crystal axis dependent measurements of coupled InAs/GaSb quantum wells' (2018), https://doi.org/10.5518/459.